Biomech Model Mechanobiol (2017) 16:439–447
DOI 10.1007/s10237-016-0828-8

ORIGINAL PAPER

Mechanics of the urethral duct: tissue constitutive formulation and structural modeling for the investigation of lumen occlusion

Arturo Nicola Natali[1,2] · Emanuele Luigi Carniel[1,2] · Chiara Giulia Fontanella[2,3] · Alessandro Frigo[1,2] · Silvia Todros[1,2] · Alessandro Rubini[2,3] · Giulia Maria De Benedictis[2,4] · Maria Angela Cerruto[5] · Walter Artibani[5]

Received: 29 April 2016 / Accepted: 31 August 2016 / Published online: 16 September 2016

Abstract Urinary incontinence, often related to sphincter damage, is found in male patients, leading to a miserable quality of life and to huge costs for the healthcare system. The most effective surgical solution currently considered for men is the artificial urinary sphincter that exerts a pressure field on the urethra, occluding the duct. The evaluation of this device is currently based on clinical and surgical competences. The artificial sphincter design and mechanical action can be investigated by a biomechanical model of the urethra under occlusion, evaluating the interaction between tissues and prosthesis. A specific computational approach to urethral mechanics is here proposed, recalling the results of previous biomechanical experimental investigation. In this preliminary analysis, the horse urethra is considered, in the light of a significant correlation with human and in consideration of the relevant difficulty to get to human samples, which anyway represents the future advance. Histological data processing allow for the definition of a virtual and a subsequent finite element model of a urethral section. A specific hyperelastic formulation is developed to characterize the nonlinear mechanical behavior. The inverse analysis of tensile tests on urethra samples leads to the definition of preliminary constitutive parameters. The parameters are further refined by the computational analysis of inflation tests carried out on the entire urethral structure. The results obtained represent, in the light of the correlation reported, a valid preliminary support for the information to be assumed for prosthesis design, integrating surgical and biomechanical competences.

Keywords Urethral duct · Tissue mechanics · Experimental testing · Computational biomechanics · Artificial urinary sphincter

✉ Arturo Nicola Natali
arturo.natali@unipd.it

1 Department of Industrial Engineering, University of Padova, Via F. Marzolo, 9, 35131 Padova, Italy

2 Centre for Mechanics of Biological Materials, University of Padova, Via F. Marzolo, 9, 35131 Padova, Italy

3 Department of Biomedical Sciences, University of Padova, Via U. Bassi, 58/B, 35131 Padova, Italy

4 Department of Animal Medicine, Production and Health, Viale dell'Università, 16, 35020 Legnaro (PD), Italy

5 Urology Clinic, Verona Integrated University Hospital, Piazzale A. Stefani, 1, 37126 Verona, Italy

1 Introduction

The biomechanical investigation of biological tissues and structures of the lower urinary system are fundamental for the comprehension of the functional response in physiological conditions. Currently, lower urinary tract dysfunctions consist of storage, voiding and post-micturition symptoms that are highly prevalent (McVary 2006) and result in a decrease in life quality (Kerrebroeck et al. 1993; Minassian et al. 2003). Incontinence affects both men and women with a significant increase depending on age (Abrams et al. 2002). However, the present work refers to male subjects, due to the specific and more complex configuration of the urethral region. In healthy conditions, the external sphincter muscle and the internal sphincter provide physiological occlusion (Brooks 2007). In case of severe incontinence (Hampel et al. 2010, prosthetic devices are applied typically in the bulbar urethra region (Aa et al. 2013). Surgical solutions include artificial urinary sphincter (Venn et al. 2000; Hussain et al. 2005; Amend et al. 2013; Wiedemann et al. 2013) and slings (Bruwaene et al. 2015). In particular, the artificial urinary sphincter is based on a cuff positioned around the urethral duct, providing lumen occlusion by an external pressure field, that can

range up to 90 cm H_2O (Hussain et al. 2005). The overall operational conditions (Venn et al. 2000) are considered during the surgical intervention. The pressure field constantly acts on urethral tissues, while is suspended when the patient releases the device for inducing micturition. Particular attention should be paid to the interaction occurring between the cuff and the urethral tissues, in consideration of potential damages as atrophy and erosion (Kim et al. 2008; Aa et al. 2013; Bates et al. 2015; Bugeja et al. 2016; Ravier et al. 2015). Complications entail surgical revision, removal and possible replacement of the device (Raj et al. 2005; Simon et al. 2005; Anusionwu and Wright 2013; Linder et al. 2015).

The mechanical functionality of the prosthetic device and the biomechanical response of urethra to imposed pressure can be approached by means of experimental and computational biomechanics investigation. Computational models of the urethra can be developed to identify the artificial sphincter pressure that ensures lumen occlusion (Marti et al. 2006) and stress and strain distributions within biological tissues (Chung 2014; Hached et al. 2014; Ramesh et al. 2014).

A preliminary computational approach to the analysis of urethra response during lumen occlusion is here proposed. The investigation recalls experimental data from a former study concerning the characterization of horse urethra samples (Natali et al. 2016). Indeed, the horse can represent a suitable animal model for ex vivo characterization, since equine urethra presents significant similarities to human one, especially concerning hystological tissue conformation (Wolfe and Moll 1999; Pozor and McDonnell 2002; Arrighi et al. 2004; Dellmann and Eurell 1998) and micturition evolutionary process (Clark et al. 1987; Ronen 1994; Brading 1999). The consideration of animal samples determines an approximation in the comparison with human case. Nonetheless, this work aims at developing a method that can be extended on the basis of an experimental investigation on human samples already in progress. The developed computational model interprets urethral tissues and structures mechanical response under intraluminal pressure and external occlusion conditions.

2 Materials and methods

2.1 Finite element model definition

Numerical model refers to results on histological conformation and experimental mechanical behavior of urethral tissues and structures, reported in a previous investigation (Natali et al. 2016). Short notes are here recalled to outline the procedure. Specimens were collected from proximal and distal regions of male horse urethras. Results from distal samples are taken into account for computational modeling, due to the similarity between horse and human urethra in this region (Pozor and McDonnell 2002; Arrighi et al. 2004). Urethral conformation and fiber distribution within tissue layers are evaluated for the definition of structural model. Urethral lumen shows a complex cross-sectional shape, ranging between slit- and star-like ones (Pullan et al. 1982). Different layers compose the urethral duct, namely a pseudostratified columnar epithelium around the lumen, a thin layer of dense connective tissue and a thick stratum of loose tissue comprising corpora spongiosa, connective septa and blood vessels (Pavlica et al. 2003). Transversal sections of urethras were collected for histological analysis and stained with Masson trichrome solution to enable the identification of different layers. Serial sectioning was carried out for an overall evaluation of tissue conformation (Natali et al. 2016) and a specific histological section is selected for the development of the model (Fig. 1), assumed in the mean position of the urethra region loaded by constant sphincteric pressure. A virtual geometrical model of urethra section is obtained from the histological image, enlarged in scale to correct shrinkage phenomena that occurred during tissue processing (Dobrin 1996). Specific image analysis routines are implemented in Matlab (The MathWorks Inc., Natick, MA, USA) aiming to geometrically characterize the conformation of urethra transversal section and to identify the different tissue layers. Median, 25th and 75th percentiles thickness values of the layers are: 0.06 [0.03, 0.08] mm, 0.14 [0.12 0.19] mm and 5.13 [4.21 5.47] mm for epithelium, dense connective tissue and lose tissue, respectively.

The geometrical model of the urethral section (Fig. 2a) is imported into the finite element preprocessing software Abaqus/CAE 6.14 (Dassault Systèmes Simulia Corp., Providence, RI). Six node triangular quadratic elements (CPS6 plane strain elements) and three node triangular linear elements (CPS3 plane strain elements) are adopted to mesh the dense connective tissue layer and the loose tissue stratum (Fig. 2b, c). Tie contact condition ensures the proper mechanical interaction at the interface between the two differently meshed regions for compatibility requirements. The mechanical contribution of the epithelial layer, due to its limited stiffness characteristics, is almost negligible. Anyway, it must be taken into account in the interaction phenomena induced by compression loads, interpreted by means of a self-contact condition. The typical nonlinear mechanical behavior of soft biological tissues suggests the assumption of an exponential pressure-overclosure relationship (Abaqus 6.14-1 Analysis User Manual, Dassault Systèmes Simulia Corp., Providence, RI). In detail, facing portions of lumen begin to interact once the clearance between them, measured in the contact normal direction, reduces to almost the double of the epithelium thickness. The contact pressure between lumen surfaces then increases exponentially as the clearance continues to diminish. When clearance approaches zero, pressure is getting to 10 kPa, in agreement with results from

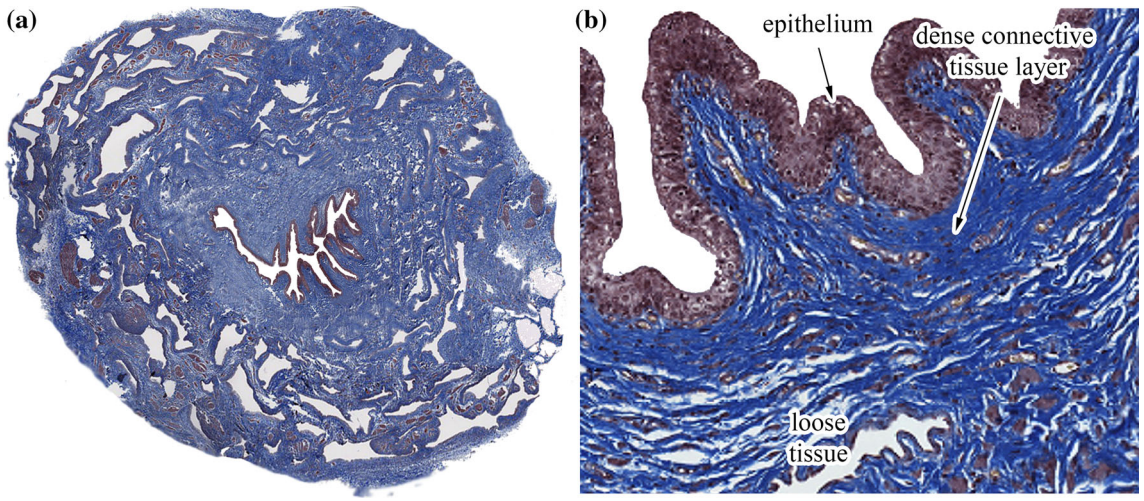

Fig. 1 Histological section from distal region of horse penile urethra (**a**); detail showing the different tissues (**b**)

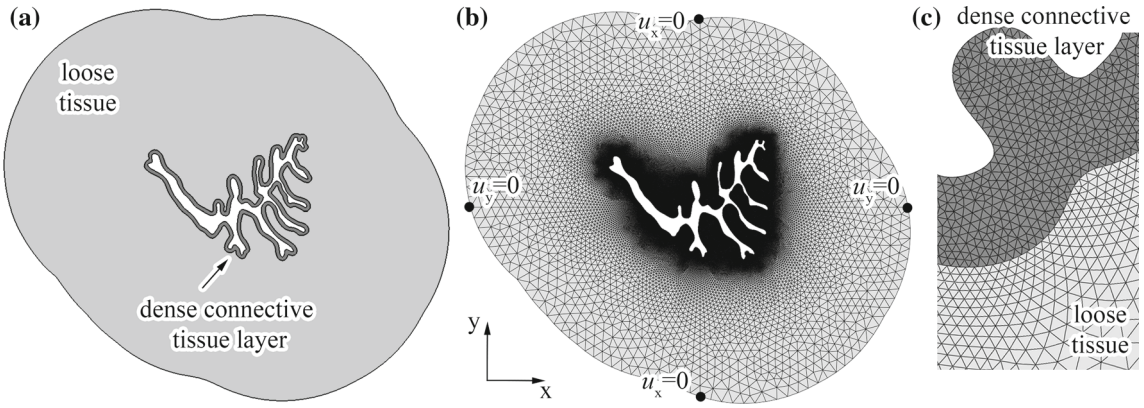

Fig. 2 Urethra geometrical model (**a**); finite element model with boundary conditions for numerical analysis of structural inflation and lumen occlusion (**b**); detail of the finite element model showing the different discretization of loose and dense tissue layers (**c**)

experimental activities on epithelial tissues (Raub et al. 2010; Chen et al. 2015). Contact frictional properties ensure the transmission of shear loads between lumen surfaces, usually fully hydrated, with a 0.02 friction coefficient (Prinz et al. 2007). Model and mesh configurations are defined through the procedures of computational mechanics. Models are developed assuming incremental mesh refinement. Numerical analyses simulating inflation tests are performed comparing the different models results, aiming to evaluate the influence of mesh conformation. Results show to be mostly affected by the size of element within the dense connective tissue layer. With regard to this region, reducing element size below 0.03 mm does not provide significant variation of results. With regard to the final configuration of the model, mean element size within the dense connective tissue layer is 0.03 mm, while it ranges between 0.03 and 0.3 mm in the loose tissue stratum. The model is composed by 31553 nodes (18142 and 13411 nodes, respectively, in dense connective layer and loose stratum) and 33695 elements (8034 and 25661 elements, respectively, in dense connective layer and loose).

2.2 Constitutive formulation

The mechanical behavior of dense connective and loose tissue is defined by a specific hyperelastic formulation that proved its capability to interpret the typical features of soft tissue mechanics in previous investigations (Natali et al. 2009, 2010; Carniel et al. 2014). The stress–strain relationship is here recalled:

$$\mathbf{P} = -p\mathbf{F}^{-T} + C_1 \exp\left[\alpha_1 \left(I_1 - 3\right)\right]\left(2\mathbf{F} - 2/3 I_1 \mathbf{F}^{-T}\right) \tag{1}$$

where $\mathbf{P}$ is the first Piola-Kirchhoff stress tensor, as a measure of nominal stress, $\mathbf{F}$ is the deformation gradient, p is a Lagrange multiplier that specifies hydrostatic pressure and

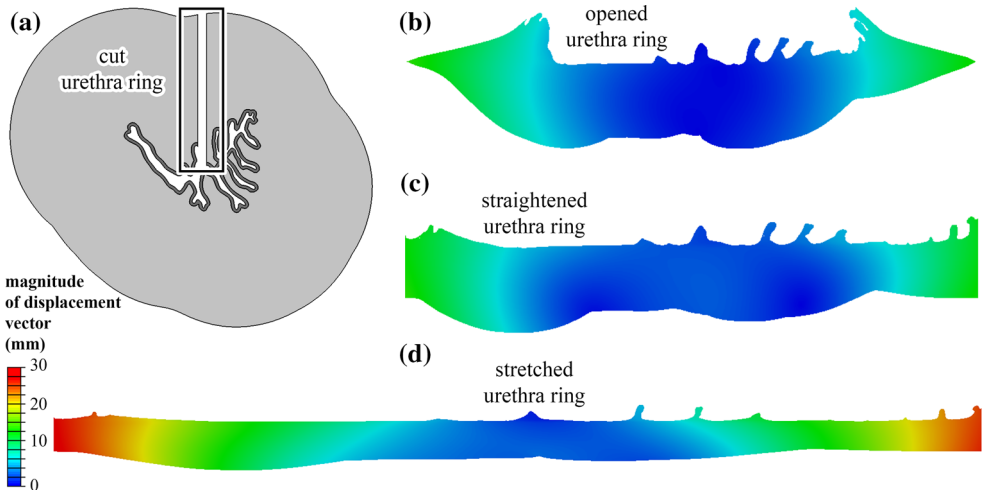

Fig. 3 Tensile tests on urethra samples. Mimicking the experimental procedure, the finite element model of the cut urethra samples (**a**) undergoes the opening (**b**) and straightening (**c**) up to large tensile stretching (**d**)

ensures the incompressibility of the material, I_1 is the first invariant of the right Cauchy-Green strain tensor $\mathbf{C} = \mathbf{F}^T\mathbf{F}$. The constitutive parameters C_1 is related to tissue shear stiffness in the unstrained configuration, while the nonlinearity parameter α_1 specifies tissue stiffening with stretch. Constitutive parameters are identified by the inverse analysis of tensile tests performed on horse urethra. Rectangular specimens (20 mm gauge-length, 5 mm width) were cut from distal urethras along circumferential directions (36 samples from thirteen male horses). Mean sample thickness was about 4 mm, as reported in Natali et al. (2016) together with additional details. A Bose® ElectroForce® (Bose Corporation, ElectroForce Systems Group, Eden Prairie, MN, USA) machine was used to perform tests. Each specimen was stretched up to 60% strain. According to the specific boundary conditions, in case of uni-axial tensile loading, the following relationships between stress and stretch components are computed from the general model (Eq. 1):

$$P_{cc} = 2C_1 \exp\left[\alpha_1\left(\lambda_c^2 + 2\lambda_c^{-1} - 3\right)\right]\left(\lambda_c - \lambda_c^{-2}\right) \qquad (2)$$

where λ_c and P_{cc} are stretch and nominal stress, respectively, along circumferential direction. Different sets of parameters are identified analyzing the statistical distribution of experimental results, as median, 25 and 75th percentiles. With regard to processing of experimental results, stretch is computed as the ratio between the gauge-length of the tissue specimen in deformed and undeformed configurations, nominal stress is evaluated as the ratio between tensile force and specimen mean cross-section area in the undeformed configuration.

The minimization of discrepancy between experimental data and model results (Natali et al. 2009) lead to the following parameters: $C_1 = 1.09[0.95, 1.37]kPa, \alpha_1 = 1.26[1.07, 1.40]$. Such parameters describe the mechanical behavior of a homogenized urethral structure. Nevertheless, tissue layers with different mechanical properties compose the urethral wall. The multi-layered configuration leads to a non-homogeneous stress and strain distribution.

A tensile test on a circumferential urethra sample is replicated by computational modeling in Fig. 3, with reference to a specific section (Fig. 3a). Finite element analysis investigates all the different steps of the experimental procedure, including urethra ring opening for the preparation of the sample (Fig. 3b), straightening as during sample gripping (Fig. 3c) and tissues stretching through tensile testing (Fig. 3d). The mechanical behavior of the tissues is defined by the specific hyperelastic formulation mentioned, which is implemented in the finite element software by a user subroutine.

Different sets of parameters must be identified for the different tissues. Experimental test faces the problem of providing specimens where different tissues are combined and their separation should induce relevant damage. To overcome this problem, the interpretation of stiffness characteristics is performed by the support of numerical model simulation. In the present case, this consideration can be referred to the coupling of dense and loose tissue with regard to the evaluation of the parameters C_1 and α_1. A numerical analysis of tensile tests is developed considering different values of a multiplier k, ranging between 1 and 1000 (Fig. 4), that represent the ratio of C_1 values attributed to the different components. The large range of k values makes it possible to evaluate a complete set of conformations of urethra tissues: $k = 1$ specifies an homogenous structure, while $k = 1000$ describe a thin and highly stiff layer surrounded by a thick and tenuous stratum.

Additional investigations are developed with regard to experimental results from inflation tests that were performed

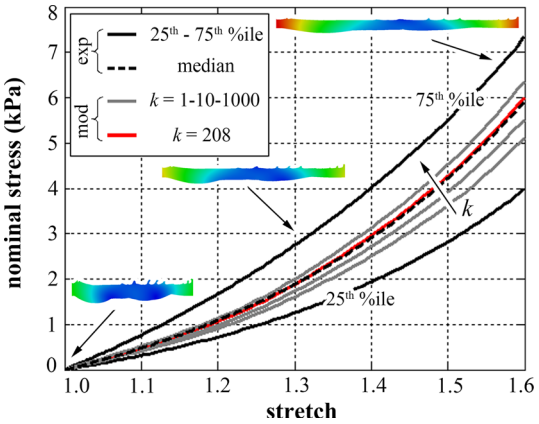

Fig. 4 Comparison of experimental and computational results from tensile tests on urethra circumferential samples. Median, 25 and 75th percentiles experimental curves are reported. Computational results are defined depending on different sets of constitutive parameters according to the values of multiplier k

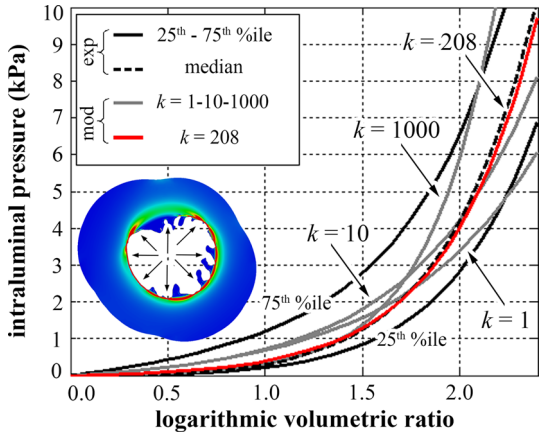

Fig. 5 Comparison of experimental and computational results from inflation tests on urethra tubular samples. Median, 25 and 75th percentiles experimental curves are reported. Computational results are defined depending on different sets of constitutive parameters according to the values of multiplier k. The logarithmic volumetric ratio is defined as the logarithm of the ratio between the volume of the urethra lumen, when mechanical action is applied and the final volume of the lumen

on urethra tubular specimens (11 distal samples from different male horses).

A homogeneous hydrostatic pressure field is applied to the intraluminal border of the urethra model. Pressure value is progressively increased to simulate the experimental progressive inflation. Null displacement conditions are imposed on four diametrically opposite nodes along single directions, on the outer boundary of the model (as shown in Fig. 2b), in order to provide minimal constraints and to satisfactorily interpret the actual constraint of the sample during experimental testing.

Different analyses are performed considering the different values of the multiplier k (Fig. 5). Numerical results from both tensile and inflation tests are compared with median experimental data. The multiplier value $k = 208$ entails the minimal overall discrepancy between computational and experimental median results. Parameters $C_1 = 34.89$ kPa, $\alpha_1 = 1.26$, and $C_1 = 0.17$ kPa, $\alpha_1 = 1.26$ are finally assumed to specify the median behavior of dense connective tissue layer and loose tissue stratum, respectively.

2.3 Numerical analysis of occlusion phenomena

The computational model interprets urethral tissues mechanical response when external occluding loads are applied. With the aim to mimic the action of artificial sphincters, a homogeneous pressure field is applied all around the external boundary of the urethral model.

The model refers to the mean section within the area where the occlusion is induced, leading to a better approximation of results in consideration of the assumption of a two dimensional model.

According to the configuration of commercial devices, the occluding pressure can reach the limit of 10 kPa, in consideration of the intraluminal pressure that ranges between 0 and 10 kPa (Griffiths 1971; Aagaard et al. 2012). Numerical analyses are performed by a two steps procedure. During the first step, the urethra is progressive inflated up to the target intraluminal pressure. During the second step, the occluding pressure is increased up to 10 kPa.

3 Results

The agreement between the experimental and computational investigations at both tissue and structure levels is reported in Figs. 4 and 5, respectively. The numerical analysis of inflation tests allows evaluating the tissues mechanical functionality when intraluminal pressure is applied. The contours of radial displacement and stress fields are reported in Figs. 6 and 7, respectively, for different values of intraluminal pressure.

Finally, urethral structure and tissues response are investigated when external occluding actions are applied. Numerical analyses that take into account different conditions, as different intraluminal pressure and occluding loads, are summarized in Fig. 8. The different curves specify the structural behavior of the urethra, as the trend of occluding pressure with lumen volume variation. Each curve pertains to a specific value of the intraluminal pressure under different compression up to occlusion and subsequent compression induced. The data are reported with regard to the volume variation depending on the load induced.

Information about tissues behavior during occlusion are reported in Fig. 9. The compressive strain field is reported

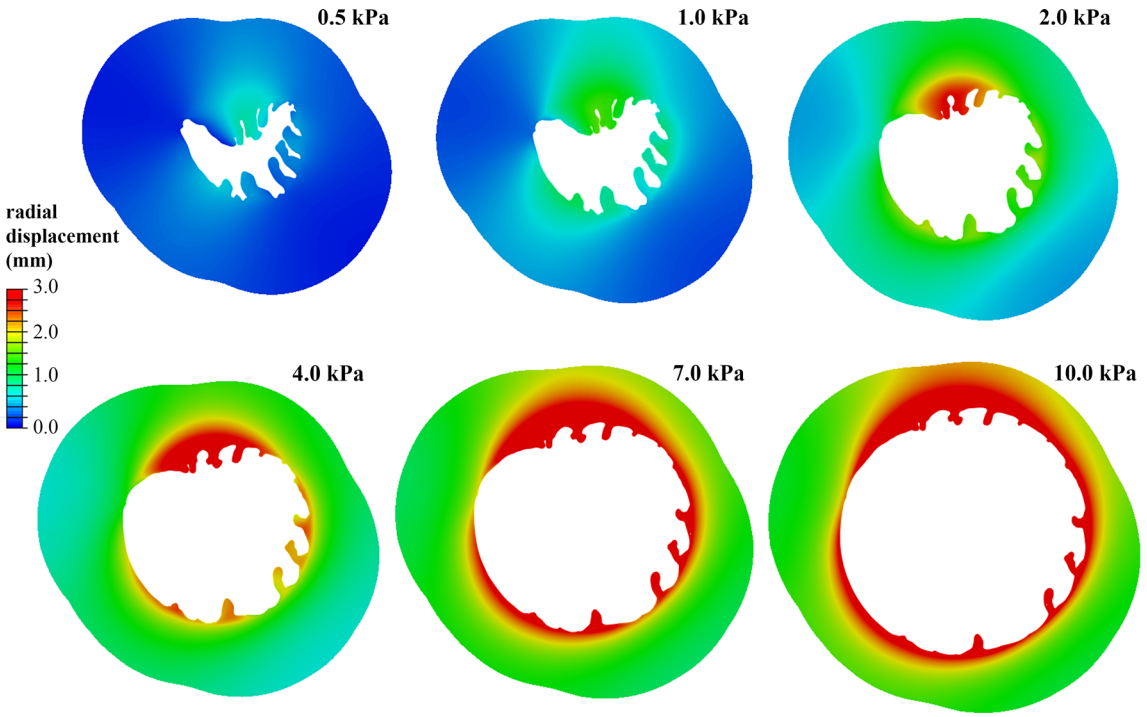

Fig. 6 Numerical analysis of structural inflation tests. Contours of radial displacement field at different intraluminal pressure conditions

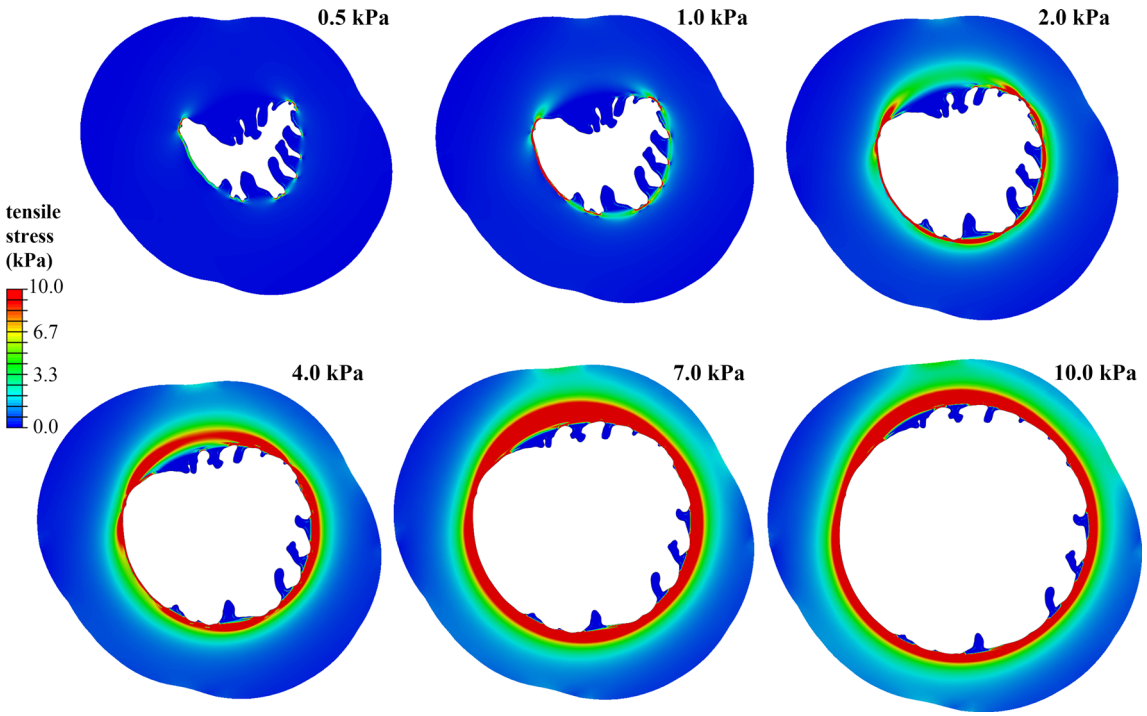

Fig. 7 Numerical analysis of structural inflation tests. Contours of tensile stress field, as the maximum principal value of the Cauchy stress tensor, at different intraluminal pressure conditions

for both loose tissue and dense connective tissue layer for different values of the occluding pressure conditions, while intraluminal pressure is 1 KPa.

4 Discussion and conclusions

The developed computational framework allows the investigation of urethral structure and tissues mechanical response

considering different configurations depending on intraluminal and occlusion pressure.

Computational analyses are performed by assuming different sets of constitutive parameters. The sets differ from one another by the multiplier k, which specifies the stiffness ratio between dense connective tissue layer and loose tissue. While the specific value of k modestly influences the tensile behavior of the urethra samples (Fig. 4), the effect on the inflation tests shows different trends and larger intensity variation (Fig. 5). In any case, the numerical results are well placed within the statistical band of experimental results for a broad range of k values. Low k values entail an almost homogenous distribution of stiffness along the urethra thickness. On the contrary, high values of k better describe the configuration of the urethra, as an inner thin and stiff layer surrounded by a thick and compliant stratum. The trend of intraluminal pressure with lumen volume significantly varies with the multiplier k, in accordance with the stiffness contribution of the dense connective tissue layer that progressively increases with the distension of the lumen. The optimal multiplier k is identified by minimizing the discrepancy between model curves and median experimental data. This assumption can be justified by considering that median data describe the average behavior of all the tested experimental samples.

As concern the tissue response in the central region within the area where the sphincteric device provides the pressure action, the accuracy of the present results can be satisfactory, in spite of the limitation that pertains to the two dimensional model conformation. This preliminary approach is justified also by the relevant computational effort determined by a highly nonlinear problem, related to material, geometry and contact conditions. The three-dimensional analysis in progress will lead to a more accurate and general interpretation of the overall response.

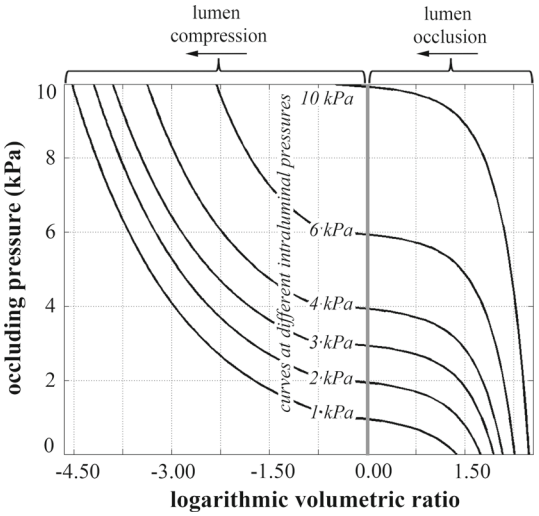

Fig. 8 Results from numerical analysis of lumen occlusion. Each curve describes the structural behavior of the urethra at a specific value of intraluminal pressure and for increasing occluding pressure conditions

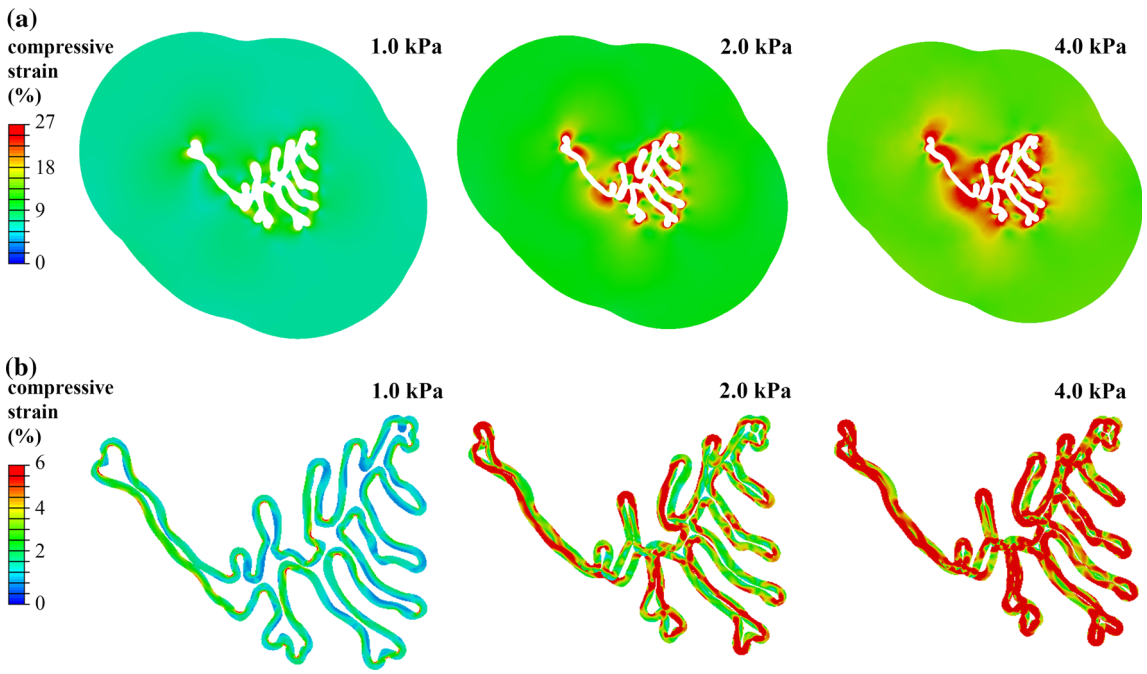

Fig. 9 Numerical analysis of lumen occlusion. Contours of compressive strain field, as the minimum principal value of the logarithmic strain tensor, into loose tissue (**a**) and dense connective layer (**b**), assuming an intraluminal pressure of 1 KPa

In general, the computational models allow the evaluation of tissues mechanical response with detail and accuracy. In Fig. 7, the stress distribution for different values of intraluminal pressure depending on urine flow (Griffiths 1971; Aagaard et al. 2012) is reported.

An interesting aspect of the analysis pertains to the tissues response when artificial sphincters, induces lumen occlusion. Fig. 8 summarizes results from numerical analyses that took into account the combination of different values of intraluminal and external occluding pressures. Occlusion occurs when external and intraluminal pressures almost equalize and subsequently urethral epithelial tissues undergo compression phenomena. Occluding actions determine substantial compressive strains within dense connective tissue and loose tissue. Artificial sphincters steadily induce such non-physiological strains within urethral tissues and potentially lead to degenerative phenomena (Hajivassiliou 1999; Garćia Montes et al. 2000; Kim et al. 2008; Aa et al. 2013; Bugeja et al. 2016).

Some notes are reported about the assumed constitutive framework. Hyperelastic formulations allow interpreting some of the typical features of soft tissue mechanics, as almost incompressible behavior and nonlinear elasticity. Biological tissues exhibit a more complex behavior and anisotropic conformation and time-dependent phenomena should be considered. For this purpose, experimental investigations are under development for a reliable identification of further parameters. Nonetheless, histological analyses (Natali et al. 2016) suggest an almost isotropic configuration of the tissues in the urethral region investigated in this work. Moderate anisotropy could just characterize the thin layer of dense connective tissue. Differently, time-dependent phenomena appear to be relevant (Natali et al. 2016) and could significantly affect stress within urethral tissues during protracted occlusive actions. This work aims just at providing a preliminary evaluation of the relationship between urethral tissues response and intensity of the occlusive action, while further investigation is in progress to better elucidate the influence of viscous effects.

As mentioned previously, additional investigation is in progress with regard also to experimental tests on human specimens and with an extension to three-dimensional model configuration. This preliminary study reports on the relevant experimental and computational effort and offers a set of results that can be considered compatible with realistic response mostly in the central region of the sphincteric cuff. In this sense, the present research can offer the basis for evaluating the relevant complexity of the problem stressing the integration of biomechanical and surgical competences that represents a fundamental term in addressing further investigation.

Acknowledgements This study has been supported by University of Padova, Project n° CPDA148900/14, titled COMPUR: Definition of COMPutational tools for the analysis of the biomechanical functionality of the lower URinary system.

Compliance with ethical standards

Conflict of interest The authors declare that they have no conflict of interest.

References

Aagaard M, Klarskov N, Sønksen J, Bagi P, Colstrup H, Lose G (2012) Urethral pressure reflectometry; a novel technique for simultaneous recording of pressure and cross-sectional area: a study of feasibility in the prostatic urethra. BJU Int 110:1178–1183

Abrams P, Cardozo L, Fall M, Griffiths D, Rosier P, Ulmstern U, van Kerrebroeck P, Victor A, Wein A (2002) The standardisation of terminology of lower urinary tract function: report from the standardisation sub-committee of the international continence society. Neurourol Urodyn 21:167–178

Amend B, Toomey P, Sievert KD (2013) Artificial sphincter. Curr Opin Urol 23:520–527

Anusionwu II, Wright EJ (2013) Indications for revision of artificial urinary sphincter and modifiable risk factors for device-related morbidity. Neurourology and Urodynamics 65:63–65

Arrighi S, Cremonesi F, Bosi G, Domeneghini C (2004) Endocrine-paracrine cells of the male urogenital apparatus: a comparative histochemical and immunohistochemical study in some domestic ungulates. Anat Histol Embryol 33:225–232

Bates AS, Martin RM, Terry TR (2015) Complications following artificial urinary sphincter placement after radical prostatectomy and radiotherapy: a meta-analysis. BJU Int 116:623–633

Brading AF (1999) The physiology of the mammalian urinary outflow tract. Exp Physiol 84:215–221

Brooks JD (2007) Anatomy of the lower urinary tract and male genitalia. In: Wein AJ, Kavoussi LR, Partin AW, Peters CA (eds) Campbell-Walsh urology, 9th edn. Saunders/Elsevier, Philadelphia, pp 38–77

Bugeja S, Ivaz SL, Frost A, Andrich DE, Mundy AR (2016) Urethral atrophy after implantation of an artificial urinary sphincter: fact or fiction? BJU International 117:669–676

Carniel EL, Gramigna V, Fontanella CG, Stefanini C, Natali AN (2014) Constitutive formulations for the mechanical investigation of colonic tissues. J Biomed Mater Res Part A 102:1243–1254

Chen J, Ahmad R, Li W, Swain M, Li Q (2015) Biomechanics of oral mucosa. J R Soc Interface 12:20150325

Chung E (2014) A state-of-the-art review on the evolution of urinary sphincter devices for the treatment of post-prostatectomy urinary incontinence: past, present and future innovations. J Med Eng Technol 38:328–332

Clark ES, Semrad SD, Bichsel P, Oliver JE (1987) Cystometrography and urethral pressure profiles in healthy horse and pony mares. Am J Vet Res 48:552–555

Dellmann HD, Eurell JA (1998) Textbook of veterinary histology, 5th edn. Lippincott, Williams & Wilkins, Baltimore

Dobrin PB (1996) Effect of histologic preparation on the cross-sectional area of arterial rings. J Surg Res 61:413–415

Garćia Montes G, Gómez Sancha F, Mundy A (2000) Artificial urinary sphincter. Archivos Españoles de Urología 53:201–210

Griffiths DJ (1971) Hydrodynamics of male micturition. I. Theory of steady flow through elastic-walled tubes. Med Biol Eng 9:581–588

Hached S, Loutochin O, Corcos J, Garon A, Sawan M (2014) Novel, remotely controlled, artificial urinary sphincter: a retro-compatible device. IEEE/ASME: Transact Mechatron 19:1352–1362

Hajivassiliou CA (1999) A review of the complications and results of implantation of the AMS artificial urinary sphincter. Eur Urol 35:36–44

Hampel C, Thuroff JW, Gillitzer R (2010) Epidemiology and etiology of male urinary incontinence. Urologe 49:481–488

Hussain M, Greenwell TJ, Venn SN, Mundy AR (2005) The current role of the artificial urinary sphincter for the treatment of urinary incontinence. J Urol 174:418–424

Kim SP, Sarmast Z, Daignault S, Faerber GJ, McGuire EJ, Latini JM (2008) Long-term durability and functional outcomes among patients with artificial urinary sphincters: a 10-year retrospective review from the University of Michigan. J Urol 179:1912–1916

Linder BJ, Piotrowski JT, Ziegelmann MJ, Rivera ME, Rangel LJ, Elliott DS (2015) Perioperative complications following artificial urinary sphincter placement. J Urol 194:716–720

Marti F, Leippold T, John H, Blunschi N, Müller B (2006) Optimization of the artificial urinary sphincter: modelling and experimental validation. Phys Med Biol 51:1361–1375

McVary K (2006) Lower urinary tract symptoms and sexual dysfunction: epidemiology and pathophysiology. BJU Int 97:23–28

Minassian VA, Drutz HP, Al-Badr A (2003) Urinary incontinence as a worldwide problem. Int J Gynecol Obstetrics 82:327–338

Natali AN, Carniel EL, Frigo A, Pavan PG, Todros S, Pachera P, Fontanella CG, Rubini A, Cavicchioli L, Avital Y, De Benedictis GM (2016) Experimental investigation of the biomechanics of urethral tissues and structures. Exp Physiol 101(5):641–656

Natali AN, Carniel EL, Gregersen H (2009) Biomechanical behaviour of oesophageal tissues: material and structural configuration, experimental data and constitutive analysis. Med Eng Phys 31:1056–1062

Natali AN, Fontanella CG, Carniel EL (2010) Constitutive formulation and analysis of heel pad tissues mechanics. Med Eng Phys 32:516–522

Pavlica P, Barozzi L, Mecnhi I (2003) Imaging of male urethra. Eur Radiol 13:1583–1596

Pozor MA, McDonnell SM (2002) Ultrasonographic measurements of accessory sex glands, ampullae, and urethra of normal stallions of various size types. Theriogenology 58:1425–1433

Prinz JF, de Wlijk RA, Huntjens L (2007) Load dependency of the coefficient of friction of oral mucosa. Food Hydrocoll 21:402–408

Pullan BR, Phillips JI, Hickey DS (1982) Urethral lumen cross-sectional shape: its radiological determination and relationship to function. BJU Int 54:399–407

Raj GV, Peterson AC, Toh KL, Webster GD (2005) Outcomes following revisions and secondary implantation of the artificial urinary sphincter. J Urol 173:1242–1245

Ramesh MV, Raj D, Sanjeevan Kalavampra V, Dilraj N, (2014) Design of wireless real time artificial sphincter control system for urinary incontinence. In: Proceedings of the IEEE international symposium on technology management and emerging technologies (ISTMET 2014), Bandung, Indonesia, pp 44–49

Raub CB, Mahon S, Narula N, Tromberg BJ, Brenner M, George SC (2010) Linking optics and mechanics in an in vivo model of airway fibrosis and epithelial injury. J Biomed Optics 15:015004

Ravier E, Fassi-Fehri H, Crouzet S, Gelet A, Abid N, Martin X (2015) Complications after artificial urinary sphincter implantation in patients with or without prior radiotherapy. BJU Int 115:300–307

Ronen N (1994) Measurements of urethral pressure profiles in the male horse. Equine Vet J 26:55–58

Simon P, Zerbib M, Debré B, Peyromaure M (2005) Results of the AMS 800 artificial urinary sphincter in men, based on a series of 47 patients. Progrès en Urologie 15:244–249

Van Bruwaene S, De Ridder D, Van der Aa F (2015) The use of sling vs sphincter in post-prostatectomy urinary incontinence. BJU Int 116:330–342

Van der Aa F, Drake MJ, Kasyan GR, Petrolekas A, Cornu J-N (2013) The artificial urinary sphincter after a quarter of a century: a critical systematic review of its use in male nonneurogenic incontinence. Eur Urol 63:681–689

Van Kerrebroeck PE, Koldewijn EL, Scherpenhuizen S, Debruyne FM (1993) The morbidity due to lower urinary tract function in spinal cord injury patients. Paraplegia 31:320–329

Venn SN, Greenwell TJ, Mundy AR (2000) The long-term outcome of artificial urinary sphincters. Clin Urol 164:702–707

Wiedemann L, Cornu JN, Haab E, Peyrat L, Beley S, Cathelineau X, Haab F (2013) Transcorporal artificial urinary sphincter implantation as a salvage surgical procedure for challenging cases of male stress urinary incontinence: surgical technique and functional outcomes in a contemporary series. BJU Int 112:1163–1168

Wolfe DF, Moll HD (1999) Large animal urogenital surgery. Williams & Wilkins, Baltimore